

Deformation of magnetic skyrmion due to skyrmion-skyrmion interaction

Zhen-Qian Cui(崔振茜), Wen-Li Yang(杨文力), and Jun-Hui Zheng(郑俊辉)
Citation: Chin. Phys. B, 2025, 34 (**7**): 077502. DOI: 10.1088/1674-1056/adca20
http://cpb.iphy.ac.cn; http://iopscience.iop.org/cpb

What follows is a list of articles you may be interested in

First- and second-order magnonic topologies in the ferromagnetic breathing SSH model modulated by non-Hermitian effects

Huasu Fu(付华宿), Lichuan Zhang(张礼川), Rami Mrad, Yuee Xie(谢月娥), and Yuanping Chen(陈元平)
Chin. Phys. B, 2025, 34 (**6**): 067506. DOI: 10.1088/1674-1056/addaa0

Multiferroicity and thermal expansion of the layered metal-organic framework $[NH_4Cl]_2[Ni(HCOO)_2(NH_3)_2]$

Dan Cheng(程丹), Yingjie He(何英杰), Shuang Liu(刘爽), Na Su(苏娜), and Young Sun(孙阳)
Chin. Phys. B, 2025, 34 (**6**): 067505. DOI: 10.1088/1674-1056/adcaa4

Influence of cooling atmosphere on the structure, magnetization, and dielectric properties of $CaBaCo_4O_7$

Gaoshang Gong(龚高尚), Minghao Wang(王明豪), Ruoshui Liu(刘若水), Yang Wu(吴杨), Lichen Wang(王利晨), Yongqiang Wang(王永强), and Baogen Shen(沈保根)
Chin. Phys. B, 2025, 34 (**4**): 047502. DOI: 10.1088/1674-1056/adbadc

Perpendicular magnetic anisotropy of $Pd/Co_2MnSi/Co/Pd$ multilayer

Xiaoqi Qin(秦晓奇), Jiaxing Tan(谭家兴), Xianwu Xiu(修显武), Wentian Cao(曹文田), and Shuyun Wang(王书运)
Chin. Phys. B, 2025, 34 (**3**): 037502. DOI: 10.1088/1674-1056/ada694

Electronic structure and coexisting topological states in ferromagnetic and antiferromagnetic phases of $MnBi_2Te_4$ quantum wires

Jian Li(李健), Zhu-Cai Yin(尹柱财), Qing-Xu Li(李清旭), and Jia-Ji Zhu(朱家骥)
Chin. Phys. B, 2025, 34 (**3**): 037501. DOI: 10.1088/1674-1056/ada551

Deformation of magnetic skyrmion due to skyrmion–skyrmion interaction

Zhen-Qian Cui(崔振茜)[1], Wen-Li Yang(杨文力)[1,2,3], and Jun-Hui Zheng(郑俊辉)[1,2,3,†]

[1] *Institute of Modern Physics and School of Physics, Northwest University, Xi'an* 710127, *China*
[2] *Shaanxi Key Laboratory for Theoretical Physics Frontiers, Xi'an* 710127, *China*
[3] *Peng Huanwu Center for Fundamental Theory, Xi'an* 710127, *China*

(Received 20 January 2025; revised manuscript received 7 April 2025; accepted manuscript online 8 April 2025)

Understanding skyrmion–skyrmion interactions and their dynamical effects is crucial for skyrmion-based applications. In this article, we investigate the deformation of skyrmions induced by the inter-skyrmion interaction in both static and dynamic scenarios for a two-skyrmion system. In the static case under a pinning magnetic field, the inter-skyrmion interaction energy decreases rapidly with increasing separation between the skyrmions, while their individual sizes grow. The semiaxis ratio of the elliptical skyrmion exhibits non-monotonic behavior, owing to the competition between skyrmion–skyrmion interactions and pinning effects. In dynamic simulations after removing the external pinning field, the two skyrmions spiral away from each other with increasing separation. Following a rapid relaxation period after magnetic field withdrawal, their semiaxis ratio typically increases with distance and the skyrmions gradually approach a perfect circular shape. These findings provide valuable insights into the behavior and interactions of two-skyrmion systems.

Keywords: ferromagnetic, skyrmion, Mumax3 software

PACS: 75.78.Cd, 75.30.Gw, 75.78.–n, 12.39.Dc

DOI: 10.1088/1674-1056/adca20 **CSTR:** 32038.14.CPB.adca20

1. Introduction

Magnetic skyrmions have attracted considerable attention since their first experimental observation in 2009.[1] These nanoscale spin textures with noncollinear magnetic order, show great promise for next-generation spintronic applications,[2–4] particularly in data storage,[5–7] owing to the following remarkable advantages. First, the small size of skyrmions enables high-density information storage.[8] Second, their topological stability ensures robustness against perturbations, making them ideal for preserving data integrity.[9] Finally, they can be efficiently driven by electric currents or electromagnetic fields, allowing for low-power data manipulation.[10,11]

In the study of skyrmion dynamics, a single skyrmion is often modeled as a rigid particle — an undeformed particle-like entity that retains its magnetic structure during motion. This assumption simplifies the description of skyrmion dynamics,[12] and consequently, the skyrmion trajectory is described by the classical Thiele equation.[13] This framework offers a phenomenological explanation for various physical phenomena, such as the skyrmion Hall effect, in which the Magnus force — proportional to the skyrmion's topological charge — drives transverse motion.[14–16] However, growing evidence from experiments and micromagnetic simulations suggests skyrmions may deviate from rigid behavior. Small currents[17–20] or interactions with defects like edges and impurities[21–24] could induce significant deformation for skyrmions. Such distortions introduce feedback in the Thiele equation, profoundly altering skyrmion motion.[25–28] The skyrmion's flexibility also enables its application in reservoir computing[29] and random number generation.[24] Recently, an improved Thiele equation incorporating deformation effects was developed, enabling precise modeling of a single skyrmion.[30]

In multi-skyrmion systems, the interaction between any two skyrmions has been empirically shown to be highly sensitive to the separation distance d. When d drops below a critical threshold, the interaction is attractive, causing the two skyrmions to merge into a single entity.[31,32] This intriguing phenomenon is a fundamental characteristic of multi-skyrmion systems and must be taken into account in the design of devices.[33] Conversely, when the separation distance exceeds this critical threshold, the interaction becomes repulsive.[34,35] In this case, the skyrmions repel each other, and the interaction potential decreases exponentially as the distance between them increases.[31,36–38] This exponential decay reveals the short-range nature of skyrmion–skyrmion interactions, thereby guaranteeing the stability of multi-skyrmion system. Recent studies have further investigated the influence of external factors such as temperature and magnetic fields on skyrmion interactions.[39–41] These factors can tune the balance between attractive and repulsive forces, thereby influencing the dynamics of skyrmions.

To explore the dynamics of multi-skyrmion systems, a straightforward approach is to generalize the Thiele equa-

†Corresponding author. E-mail: junhui.zheng@nwu.edu.cn

© 2025 Chinese Physical Society and IOP Publishing Ltd. All rights, including for text and data mining, AI training, and similar technologies, are reserved.

tion to describe the kinetics of multi-skyrmions. As a first step towards this goal, it is necessary to characterize both the skyrmion–skyrmion interaction and the resulting deformation of skyrmions. In this article, we investigate the deformation of skyrmions arising from their interactions, from both static and dynamic perspectives. First, we analyze the static skyrmion profile under external magnetic fields, which are used to pin the skyrmions. We aim to elucidate how the inter-skyrmion distance and external magnetic fields deform the skyrmion profiles, which would further affect their dynamics and mutual interactions. Second, we focus on the dynamic skyrmion profile during the evolution of two interacting skyrmions. Here, we characterize the repulsion-induced deformation and motion of the interacting skyrmions, providing a comprehensive view of their dynamic behavior. Unlike previous studies focusing on skyrmion deformation induced by external fields or defects, our work specifically highlights the effects of skyrmion–skyrmion interactions. We characterize the $m_z = 0$ contour using an ellipse, whose geometry is described by its semiaxes and their ratio. This ratio exhibits a non-monotonic dependence on skyrmion distance, resulting from the competition between inter-skyrmion interactions and pinning effects in static systems. For dynamic systems, while the Thiele equation typically describes the kinetics of a single skyrmion under external fields, our study reveals self-driving behaviors in bi-skyrmion systems arising from inter-skyrmion interactions. The size and the ratio of the semiaxes increase (after relaxation) during the spiral motion of the two skyrmions, which is caused by their repulsive interaction. These insights into skyrmion interactions and deformation should advance the development of equations of motion for bi-skyrmion and multi-skyrmion systems. The remainder of this article is structured as follows: the model is presented in Section 2, the numerical simulations and analysis are shown in Section 3, and a brief conclusion is provided in Section 4.

2. System and model

We investigate a Néel-type skyrmion system in a thin film (such as Pd/Fe/Ir, and Pt/Co) that exhibits the Dzyaloshinskii–Moriya interaction (DMI).[7,15] The Hamiltonian, within the framework of a continuous model, is given by the following equation:

$$E = T\iint \left[A|\nabla \boldsymbol{m}|^2 + D(m_z \nabla\cdot \boldsymbol{m} - \boldsymbol{m}\cdot\nabla m_z) - K(m_z)^2 - M_s B(1-m_z)\right] \mathrm{d}x\mathrm{d}y, \tag{1}$$

where T denotes the material thickness and $\boldsymbol{m}$ represents the unit vector of the magnetization field. The four terms in Eq. (1) correspond to the Heisenberg interaction energy, the DMI energy, the magnetocrystalline anisotropy, and the Zeeman energy, respectively.[42]

The dynamics of the local magnetization is governed by the Landau–Lifshitz–Gilbert (LLG) equation

$$\partial_t \boldsymbol{m} = -\gamma_e \boldsymbol{m}\times \boldsymbol{H}_{\mathrm{eff}} + \alpha \boldsymbol{m}\times\partial_t \boldsymbol{m}, \tag{2}$$

where γ_e is the gyromagnetic ratio and α is the Gilbert damping parameter. In our numerical simulations, we utilize the Mumax3 package to solve the LLG equation.[43,44] Analytically, for an isolated skyrmion case, one could employ polar coordinates to describe the magnetization $\boldsymbol{m} = (\sin\Theta\cos\Phi, \sin\Theta\sin\Phi, \cos\Theta)$, where Θ and Φ are functions of the polar coordinates (r,ϕ) of the position in the real space. When the skyrmion is situated at the center (the origin of the coordinate system), the stable magnetic moment at a given position can be expressed as $\Theta = \Theta(r)$ and $\Phi(\phi) = \nu\phi + \gamma$. In this context, $\nu = \pm 1$ refers to a skyrmion and an antiskyrmion, respectively. Moreover, $\gamma = 0$ or π corresponds to a Néel-type skyrmion, while $\gamma = \pm\pi/2$ represents a Bloch-type of skyrmion. Taking $\nu = 1$ as an example, from the trial function

$$\Theta(r) = 2\arctan\left[\frac{\sinh(R/w)}{\sinh(r/w)}\right], \tag{3}$$

one can determine the radius of the skyrmion (R) and the wall width (w) of the skyrmion by minimizing the total energy [Eq. (1)].[42] The approximate result is

$$R = \frac{\pi D\sqrt{A}}{\sqrt{16AK^2 - \pi^2 D^2 K}}. \tag{4}$$

Note that at the position $r = R$, one has $\Theta = \pi/2$ and $m_z = 0$. From the $m_z = 0$ isohypse line contour, the isolated skyrmion exhibits a circular morphology. However, when two skyrmions approach each other, their profiles undergo significant deformation, breaking the rotational symmetry characteristic of isolated skyrmions.

3. Results

3.1. Two static skyrmion profiles

In ferromagnetic thin films with DMI, skyrmions and skyrmion lattices can emerge and achieve stability under the influence of suitably applied magnetic fields. Experimentally, a microscopic magnetic tip, which generates a local out-of-plane magnetic field, has been effectively utilized to catalyze the nucleation of skyrmions.[45] To delve into the intricacies of how skyrmion interactions affect the profiles of these magnetic entities, we consider the two-magnetic-tip case. We model the impact of these two tips as two uniform local out-of-plane magnetic fields, each confined to a disk-shaped region. As depicted in Fig. 1(a), the m_z configuration represents the initial state prior to any relaxation processes. Within these two disk regions, the uniform magnetic field is set as $\boldsymbol{B} = B\boldsymbol{e}_z$ with $B = 5$ T, and the magnet moments are polarized such that $m_z = 1$, which is in direct opposition to the magnetization in the surrounding outer region. The diameter of the disks is denoted as l, while the distance separating the centers of the two disks is represented by d.

To observe the formation of the two skyrmions, we employ micromagnetic simulations. The material parameters are set as follows. The film size is chosen to be 256 nm × 256 nm × 0.5 nm. The system's length and width are sufficiently large to effectively mitigate boundary effects. The cell size is set at 0.5 nm × 0.5 nm × 0.5 nm, ensuring a fine resolution for the simulation. The simulation uses a grid lattice of $512 \times 512 \times 1$. The Heisenberg exchange constant is $A = 1.5 \times 10^{-11}$ J/m, the DMI constant is $D = 3.5 \times 10^{-3}$ J/m^2, the saturation magnetization is $M_s = 5.8 \times 10^5$ A/m, and the easy-axis anisotropic exchange coupling constant is $K = K_u - \mu_0 M_s^2/2$ with $K_u = 0.8 \times 10^6$ J/m^3.[42]

Leveraging the Mumax3 package, we numerically solve the LLG equation.[42,46,47] In our simulation, the Gilbert damping parameter is set as $\alpha = 0.03$. Previous research has revealed a critical distance between two skyrmions. If two skyrmions are closer than this threshold, they rapidly merge into a single entity.[31,32] This critical value depends on the disk diameter and the magnetic field strength.[39] When the two regions are sufficiently separated, the resulting two skyrmions are stable. After relaxation, the skyrmion configurations are shown in Fig. 1(b). These two skyrmions are pinned by the external magnetic field from the tips.

We define the skyrmion centers as the local maxima of the m_z component. To numerically determine the skyrmion centers with high precision, we implement the following procedure: First, we identify the two local maxima among the discretized grid points. Next, we perform quadratic fitting along the x- and y-axes, respectively, to obtain refined center coordinates. After determining the skyrmion centers $\boldsymbol{r}_1$ and $\boldsymbol{r}_2$, we define the skyrmion separation distance as $d_s \equiv |\boldsymbol{r}_1 - \boldsymbol{r}_2|$. Due to the repulsive interaction between the skyrmions, the skyrmion centers are displaced from the centers of the magnetic field (the disk centers), resulting in $d_s \geq d$. As illustrated in Fig. 1(c), d_s increases monotonically with d, and the two values converge when d becomes sufficiently large.

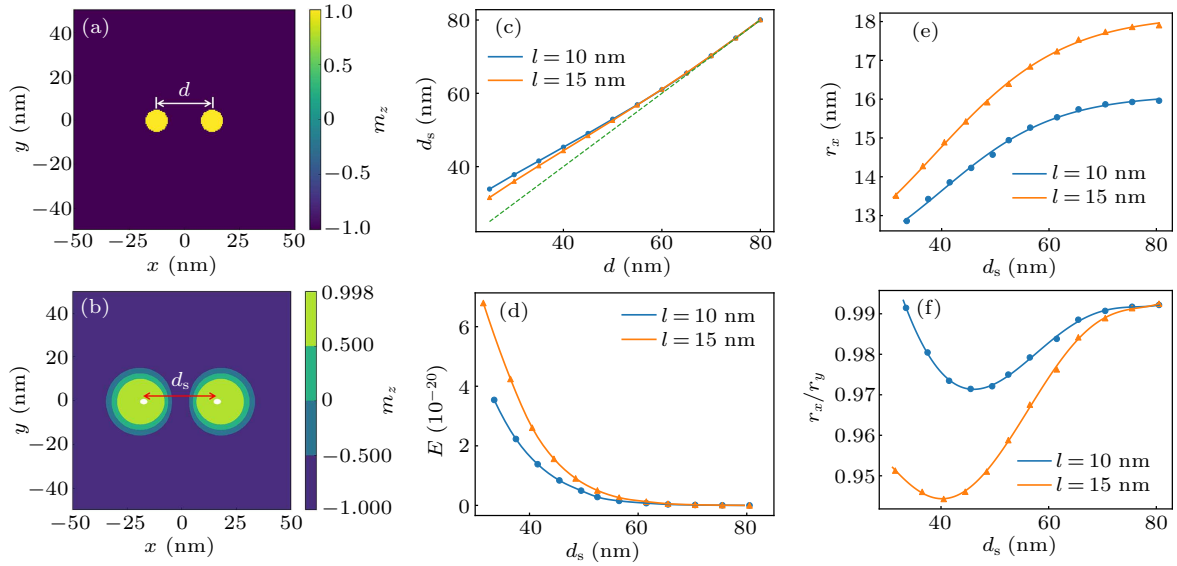


Fig. 1. (a) In the disk regions, the magnetic fields are set as $B = 5$ T, and the initial magnetization is set as $m_z = 1$ in the disks and $m_z = -1$ out of the regions. d labels the distance between the two disk centers. (b) The magnetization distribution m_z after relaxation. d_s marks the distance between the two peaks of the m_z in the two skyrmions. (c) The skyrmion distance as a function of the disk distance. The dotted green line refers to the function $d_s = d$. (d) The skyrmion interaction energy as a function of the skyrmion distance. (e) The length of the semiaxis along the x direction, r_x, as a function of the skyrmion distance d_s. (f) The ratio r_x/r_y as a function of the skyrmion distance. (a)–(b) The disk diameter is $l = 10$ nm. (c)–(f) The symbols represent numerical simulation results for disk diameters of $l = 10$ nm and 15 nm, and the solid lines are the corresponding fitting lines.

Upon removal of the initial local magnetic fields $\boldsymbol{B}$, the two skyrmions exhibit mutual repulsion. We calculate the total energy of the two-skyrmion system at the instant time when the initial local magnetic fields are withdrawn. At this moment, the skyrmions maintain their original profiles while the Zeeman energy (contributed by the coupling with the field $\boldsymbol{B}$) is excluded from consideration. The interaction energy between two skyrmions at absolute zero temperature is defined as the energy difference relative to the system's total energy when the two skyrmions are infinitely separated. That is to say, when the distance between skyrmions is very large ($d_s \to \infty$), there is no interaction between them, and the increased energy as the distance decreases is identified as the interaction energy.[40] The resultant interaction energy is graphically represented in Fig. 1(d), and it quantitatively aligns with the exponential relationship $E(d) \propto \exp(-d_s/\lambda)$.[31,36–39] The parameter $1/\lambda$, which denotes the rate of this exponential decay, is influenced by the disk diameter and the field strength B, as the initial local magnetic fields can alter the skyrmion profiles.

The interaction between skyrmions induces deformation of the skyrmion, which in turn alters the interaction. The final skyrmion profile is obtained by minimizing the total energy in the presence of the initial local magnetic fields. To examine the deformation of the skyrmion, we analyze the isohypse line where $m_z = 0$. In the case of an isolated skyrmion, this isohypse line forms a perfect circle, with the radius serving as an

indicator of the skyrmion size. However, when two skyrmions are present, the isohypse line $m_z = 0$ for each skyrmion takes on an elliptical shape. We denote the length of the semiaxis along the x direction as r_x. In Fig. 1(e), we plot the averaged r_x of the two skyrmions as a function of d_s. It is clear that the skyrmion size increases progressively with the distance between them, eventually reaching a constant value when the distance is substantially large. The disk diameter significantly influences the maximum skyrmion radius. This asymptotic value represents the size of an isolated skyrmion when a magnetic field is present within a disk. Note that in the absence the magnetic field, an isolated skyrmion in the current parameter set has a radius of $R = 15.5$ nm in the numerical simulation [the approximated result is $R = 12.35$ nm based on Eq. (4)]. From the asymptotic values shown in Fig. 1(e), we conclude that the presence of the magnetic field in the disk expands the skyrmion.

In two-skyrmion systems, the length of the semiaxis along the y direction (r_y) no longer matches that along the x direction (r_x). The ratio r_x/r_y as a function of d_s is shown in Fig. 1(f). These ratios approach 1 when d_s is extremely large, indicating a return to a perfect circular shape. As the distance d_s decreases from infinity, the ratio r_x/r_y diminishes due to stronger skyrmion repulsion. However, when d_s reaches a critical value, further decreases in d_s unexpectedly cause the ratio r_x/r_y to increase. This seemingly contradictory phenomenon arises from the pinning effect of the magnetic field. In such case, the deviation between the skyrmion center and disk center increases, causing the local magnetic fields to exert a dragging force on the skyrmion. This force counteracts the inter-skyrmion repulsion, stretching the skyrmion along the x-direction and thus increasing the ratio.

3.2. Bi-skyrmion motion

We now examine the deformation of skyrmions during dynamical evolution in a two-skyrmion system. When external magnetic fields are removed, the two skyrmions become free and evolve into quasi-particles. The distance between them increases progressively due to their repulsive interaction. Owing to their topological nature, the skyrmions do not simply move apart in a straight line but instead follow helicoidal trajectories around each other.

To track the trajectory of the skyrmions, we identify the two local maximum points of m_z, using the method described in the previous subsection. The relative position vector between the two skyrmion centers is given by $\boldsymbol{r} = \boldsymbol{r}_1 - \boldsymbol{r}_2 \equiv d_s(\cos\theta, \sin\theta)$, where $d_s = |\boldsymbol{r}|$ is the distance between the skyrmions and θ is the polar angle of $\boldsymbol{r}$. In Figs. 2(a) and 2(b), we present d_s and θ as functions of time t during the dynamical evolution for different sets of parameters, including material thickness $T = 0.4$ nm and $T = 0.5$ nm, disk distance $d = 25$ nm and $d = 35$ nm, and magnetic field strength $B = 5$ T and $B = 2.5$ T. The distance d_s increases with time, but the rate of increase decelerates because the interaction between the skyrmions weakens with increasing separation. Meanwhile, the monotonic decrease in θ serves as evidence of the spiral motion of the two skyrmions, with their rotation rate also diminishing over time. To illustrate this spiral motion, we plot the trajectory of $\boldsymbol{r}$ in Fig. 2(c). The chirality of the spiral motion is determined by the skyrmion's topology (the winding number), which depends on the relative orientation of the skyrmion's central magnetization compared to the surrounding magnetization. Note that the distance between skyrmions almost grows linearly with the polar angle, as clearly depicted in Fig. 2(d).

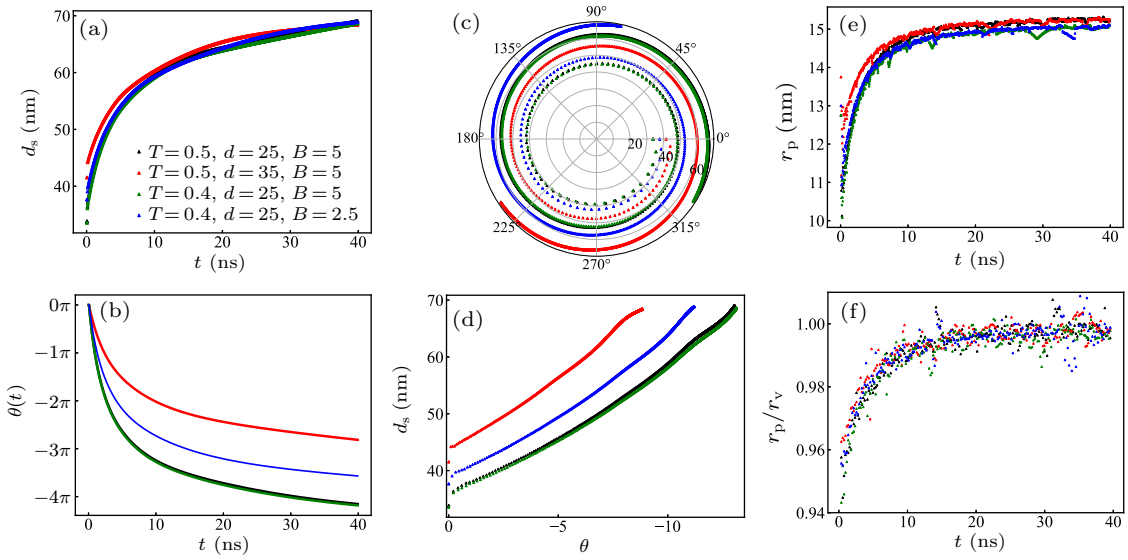


Fig. 2. (a) Skyrmion distance d_s and (b) relative azimuth angle θ as a function of time t in the dynamical evolution. (c) The trajectory of the relative position $\boldsymbol{r} = \boldsymbol{r}_1 - \boldsymbol{r}_2$ between the two skyrmions. The time interval for the two neighboring points is 0.04 ns. (d) Skyrmion distance d_s as a function of relative azimuth angle θ in the dynamical evolution. (e) The skyrmion semiaxis lengths as functions of time t in the dynamical evolution. (f) The ratio r_p/r_v as a function of time t. In these simulations, the initial skyrmions are created using the magnetic tips with disk radius $l = 10$ nm. Panels (a)–(f) use a common legend shown in panel (a). The units in the legend are nm (nanometers) for thickness T and distance d, and Tesla for the magnetic field B.

To characterize the profile of the skyrmions during their dynamical evolution, we define two unit vectors as shown in Fig. 3(b): $\boldsymbol{n}_1(t) = \boldsymbol{r}/|\boldsymbol{r}|$ and $\boldsymbol{n}_2(t)$, where $\boldsymbol{n}_1$ is parallel to $\boldsymbol{r}$ and $\boldsymbol{n}_2$ is perpendicular to $\boldsymbol{n}_1$. One of the two skyrmions stays in the region of $\mathcal{R}_1 \equiv \{\boldsymbol{R}|\boldsymbol{R}\cdot\boldsymbol{n}_1 > 0 \text{ and } m_z > 0\}$, where $\boldsymbol{R}$ represents the position of the magnets, while the other one is in the region of $\mathcal{R}_2 \equiv \{\boldsymbol{R}|\boldsymbol{R}\cdot\boldsymbol{n}_1 < 0 \text{ and } m_z > 0\}$. Next, we calculate the projections $V_2 = \boldsymbol{R}\cdot\boldsymbol{n}_2$ and $V_1 = \boldsymbol{R}\cdot\boldsymbol{n}_1$ for all $\boldsymbol{R}$ in each region. For each skyrmion, the semiaxis along $\boldsymbol{n}_1$ is defined as

$$r_{\mathrm{p}} = \left(\max\{V_1\}_{\mathcal{R}_i} - \min\{V_1\}_{\mathcal{R}_i}\right)/2, \tag{5}$$

and the semiaxis along $\boldsymbol{n}_2$ is defined as

$$r_{\mathrm{v}} = \left(\max\{V_2\}_{\mathcal{R}_i} - \min\{V_2\}_{\mathcal{R}_i}\right)/2, \tag{6}$$

respectively, where $i = 1, 2$. Given the presence of two skyrmions, in Fig. 2(e), we plot the averaged r_{p} of the two skyrmions as functions of time t. It is evident that immediately after the removal of the local magnetic field in the disks, the shape of the skyrmion oscillates severely, which is significantly different from the elliptical shape before about 0.2 ns. The semiaxes defined above, r_{p}, as well as r_{v}, experience a short-time chaos (with a large oscillation) and then gradually grow over time. The observed chaos in the semiaxis lengths, lasting approximately 0.2 ns, is related to the relaxation dynamics of the skyrmions. By comparing the chaos period to the relaxation time for initial preparation of the two-skyrmion system, we confirm that they are of the same order of magnitude. After a sufficiently long period of evolution, the two skyrmion reach a stable size (the isolated skyrmion size). Moreover, as shown in Fig. 2(f), the ratio $r_{\mathrm{p}}/r_{\mathrm{v}}$, after relaxation, gradually increases towards 1, indicating that the skyrmions approach a circular profile. However, there are notable noises here, which are attributed to the inherent precision limitations to identifying the boundary of the skyrmions ($m_z = 0$) in the discrete lattices. Another reason is that the axes of the ellipse do not exactly coincide with the $\boldsymbol{n}_1$ and $\boldsymbol{n}_2$ directions.

In the dynamic simulations, we choose two different thicknesses. Increasing the material thickness enhances the system's energy (see Eq. (1)), thereby strengthening the skyrmion repulsion. However, it does not qualitatively alter the results as shown in Fig. 2. Decreasing the magnetic field strength weakens the pinning effect, leading to increased deviation of d_{s} with respect to d. Consequently, the initial skyrmion separation increases, similar to the effect of increasing the disk distance d, as shown in Fig. 2(a). These adjustments modify the two-skyrmion system's initial state, including both separation distance and skyrmion shape. However, after relaxation, the evolution of axes and their ratio remain qualitatively consistent. The initial rapid changes in size and shape, followed by a gradual stabilization, highlight the complex interplay between the internal magnetic structure of the skyrmions and the interaction between skyrmions.

In Fig. 3, we also plot the skyrmion profile at several distinct moments in time to provide a visual representation of these dynamic changes, offering a glimpse into the skyrmion deformation.

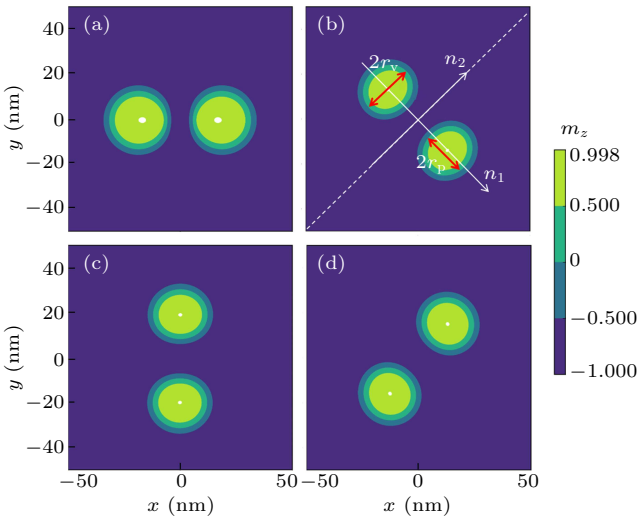


Fig. 3. The real-space distribution of the z-component magnetic moment, m_z, in the dynamic evolution process when (a) $t = 0$ ns, (b) $t = 0.24$ ns, (c) $t = 0.44$ ns, and (d) $t = 0.64$ ns. The skyrmions rotate clockwise.

4. Conclusion

We have studied the static characteristics and unconstrained dynamic behavior in two-skyrmion systems. For the static case, magnetic tips are used to create two skyrmions. We analyze the relationship between inter-skyrmion interaction energy, the semiaxis of the skyrmions, and the ratios of these semiaxis with respect to the skyrmion distance. The interaction energy quickly decreases with the distance, demonstrating the short-ranged nature of the interaction. In contrast, the size of the skyrmion grows due to the weakening of the inter-skyrmion interaction. However, the ratio of the semiaxis shows a non-monotonic behavior, which arises from the competition between the skyrmion–skyrmion interaction and the pinning effect from the local magnetic field. For dynamics, we simulate the evolution of skyrmions without external constraints. The two skyrmions move in a 2D spiral trajectory with increasing distance. For larger distances, the velocity is smaller. Typically, the ratio of the semiaxis increases with the distance. However, at the beginning of the withdrawal of the magnetic field, the skyrmion shape changes with a significant oscillation during the relaxation.

In summary, this study clarifies the relationship between skyrmion distance and interaction energy, and explores their impact on skyrmion shape in both static cases and dynamic processes. It would provide a means to investigate

how skyrmion deformation affects skyrmion motion in multi-skyrmion systems, going beyond the rigid-shape assumption used in Thiele's equation.

Acknowledgements

Project supported by the National Natural Science Foundation of China (Grant Nos. 12175180, 11934015, and 12247103, Shaanxi Fundamental Science Research Project for Mathematics and Physics (Grant Nos. 22JSZ005 and 22JSQ041), and the Natural Science Basic Research Program of Shaanxi Province, China (Grant No. 2024JC-YBMS-022).

References

[1] Mühlbauer S, Binz B, Jonietz F, Pfleiderer C, Rosch A, Neubauer A, Georgii R and Böni P 2009 *Science* **323** 915
[2] Rößler U K, Bogdanov A N and Pfleiderer C 2006 *Nature* **442** 797
[3] Yu X Z, Onose Y, Kanazawa N, Park J H, Han J H, Matsui Y, Nagaosa N and Tokura Y 2010 *Nature* **465** 901
[4] Onose Y, Okamura Y, Seki S, Ishiwata S and Tokura Y 2012 *Phys. Rev. Lett.* **109** 037603
[5] Fert A, Cros V and Sampaio J 2013 *Nat. Nanotechnol.* **8** 152
[6] Fert A, Reyren N and Cros V 2017 *Nat. Rev. Mater.* **2** 17031
[7] Romming N, Hanneken C, Menzel M, Bickel J E, Wolter B, von Bergmann K, Kubetzka A and Wiesendanger R 2013 *Science* **341** 636
[8] Heinze S, von Bergmann K, Menzel M, Brede J, Kubetzka A, Wiesendanger R, Bihlmayer G and Blügel S 2011 *Nat. Phys.* **7** 713
[9] Nagaosa N and Tokura Y 2013 *Nat. Nanotechnol.* **8** 899
[10] Yu X Z, Kanazawa N, Zhang W Z, Nagai T, Hara T, Kimoto K, Matsui Y, Onose Y and Tokura Y 2012 *Nat. Commun.* **3** 988
[11] Luo J, Guo J H, Hou Y H, Wang J L, Xu Y B, Zhou Y, Pong P W T and Zhao G P 2023 *Chin. Phys. Lett.* **40** 097501
[12] Iwasaki J, Mochizuki M and Nagaosa N 2013 *Nat. Commun.* **4** 1463
[13] Thiele A A 1973 *Phys. Rev. Lett.* **30** 230
[14] Litzius K, Lemesh I, Krüger B, Bassirian P, Caretta L, Richter K, Büttner F, Sato K, Tretiakov O A, Förster J, Reeve R M, Weigand M, Bykova I, Stoll H, Schütz G, Beach G S D and Kläui M 2017 *Nat. Phys.* **13** 170
[15] Jiang W, Zhang X, Yu G, Zhang W, Wang X, Jungfleisch M B, Pearson J E, Cheng X, Heinonen O, Wang K L, Zhou Y, Hoffmann A and te Velthuis S G E 2017 *Nat. Phys.* **13** 162
[16] Neubauer A, Pfleiderer C, Binz B, Rosch A, Ritz R, Niklowitz P G and Böni P 2009 *Phys. Rev. Lett.* **102** 186602
[17] Juge R, Je S G, de Souza Chaves D, Buda-Prejbeanu L D, Peña-Garcia J, Nath J, Miron I M, Rana K G, Aballe L, Foerster M, Genuzio F, Mentes T O, Locatelli A, Maccherozzi F, Dhesi S S, Belmeguenai M, Roussigné Y, Auffret S, Pizzini S, Gaudin G, Vogel J and Boulle O 2019 *Phys. Rev. Appl.* **12** 044007
[18] Litzius K, Leliaert J, Bassirian P, Rodrigues D, Kromin S, Lemesh I, Zazvorka J, Lee K J, Mulkers J, Kerber N, Heinze D, Keil N, Reeve R M, Weigand M, Van Waeyenberge B, Schütz G, Everschor-Sitte K, Beach G S D and Kläui M 2020 *Nat. Electron.* **3** 30
[19] Ritzmann U, von Malottki S, Kim J-V, Heinze S, Sinova J and Dupé B 2018 *Nat. Electron.* **1** 451
[20] Yasin F S, Masell J, Karube K, Kikkawa A, Taguchi Y, Tokura Y and Yu X 2022 *Proc. Natl. Acad. Sci. USA* **119** e2200958119
[21] Lima Fernandes I, Bouaziz J, Blügel S and Lounis S 2018 *Nat. Commun.* **9** 4395
[22] Reichhardt C, Reichhardt C J O and Milošević M V 2022 *Rev. Mod. Phys.* **94** 035005
[23] Gruber R, Zázvorka J, Brems M A, Rodrigues D R, Dohi T, Kerber N, Seng B, Vafaee M, Everschor-Sitte K, Virnau P and Kläui M 2022 *Nat. Commun.* **13** 3144
[24] Wang K, Zhang Y, Bheemarasetty V, Zhou S, Ying S C and Xiao G 2022 *Nat. Commun.* **13** 722
[25] Büttner F, Moutafis C, Schneider M, Krüger B, Günther C M, Gellhufe J, von Korff Schmising C, Mohanty J, Pfau B, Schaffert S, Bisig A, Foerster M, Schulz T, Vaz C A F, Franken J H, Swagten H J M, Kläui M and Eisebitt S 2015 *Nat. Phys.* **11** 225
[26] Liu L, Chen W and Zheng Y 2022 *Phys. Rev. Lett.* **128** 257201
[27] Roy P E, Otxoa R M and Moutafis C 2019 *Phys. Rev. B* **99** 094405
[28] Ribeiro de Assis I, Mertig I and Göbel B 2023 *Phys. Rev. B* **108** 144438
[29] Pinna D, Bourianoff G and Everschor-Sitte K 2020 *Phys. Rev. Appl.* **14** 054020
[30] Liu L, Chen W and Zheng Y 2023 *Phys. Rev. Lett.* **131** 246701
[31] Capic D, Garanin D A and Chudnovsky E M 2020 *J. Phys.: Condens. Matter* **32** 415803
[32] Tiwari K L, Lavoie J, Pereg-Barnea T and Coish W A 2019 *Phys. Rev. B* **100** 125414
[33] Zhang X, Ezawa M and Zhou Y 2015 *Sci. Rep.* **5** 9400
[34] Sommermann H M, Wyld H W and Pethick C J 1985 *Phys. Rev. Lett.* **55** 476
[35] Jackson A, Jackson A D and Pasquier V 1985 *Nucl. Phys. A* **432** 567
[36] Brearton R, van der Laan G and Hesjedal T 2020 *Phys. Rev. B* **101** 134422
[37] Kutschera M and Pethick C J 1985 *Nucl. Phys. A* **440** 670
[38] Kaulfuss U B and Meissner U G 1985 *Phys. Rev. D* **31** 3024
[39] Wang Y, Wang J, Kitamura T, Hirakata H and Shimada T 2022 *Phys. Rev. Appl.* **18** 044024
[40] Wang Y, Wang J, Kitamura T, Hirakata H and Shimada T 2024 *Int. J. Mech. Sci.* **261** 108699
[41] Du H, Zhao X, Rybakov F N, Borisov A B, Wang S, Tang J, Jin C, Wang C, Wei W, Kiselev N S, Zhang Y, Che R, Blügel S and Tian M 2018 *Phys. Rev. Lett.* **120** 197203
[42] Wang X S, Yuan H Y and Wang X R 2018 *Commun. Phys.* **1** 31
[43] Zhang S and Li Z 2004 *Phys. Rev. Lett.* **93** 127204
[44] Vansteenkiste A, Leliaert J, Dvornik M, Helsen M, Garcia-Sanchez F and van Waeyenberge B 2014 *AIP Advances* **4** 107133
[45] Zhang S, Zhang J, Zhang Q, Barton C, Neu V, Zhao Y, Hou Z, Wen Y, Gong C, Kazakova O, Wang W, Peng Y, Garanin D A, Chudnovsky E M and Zhang X 2018 *Appl. Phys. Lett.* **112** 132405
[46] Exl L, Bance S, Reichel F, Schrefl T, Stimming H P and Mauser N J 2014 *J. Appl. Phys.* **115** 17D118
[47] Mulkers J, van Waeyenberge B and Milošević M V 2017 *Phys. Rev. B* **95** 144401